Deep-Learning Based Reconfigurable Intelligent Surfaces for Intervehicular Communication

Bulent Sagir, Erdogan Aydin, and Haci Ilhan, *Senior Member, IEEE*

***Abstract*—This paper proposes a novel deep neural network (DNN) assisted cooperative reconfigurable intelligent surface (RIS) scheme and a DNN-based symbol detection model for intervehicular communication. In the considered realistic channel model, the channel links between moving nodes are modeled as cascaded Nakagami-m channels, and the links involving any stationary node are modeled as Nakagami-m fading channels, where all nodes between source and destination are realized with RIS-based relays. The performances of the proposed models are evaluated and compared against the conventional methods in terms of bit error rate (BER) and computational complexity. It is shown that the proposed DNN-based systems achieve almost the same performance as conventional systems with low system complexity.**

***Index Terms*—Deep neural networks (DNN), reconfigurable intelligent surface (RIS), deep learning (DL), cooperative communication, intervehicular communication.**

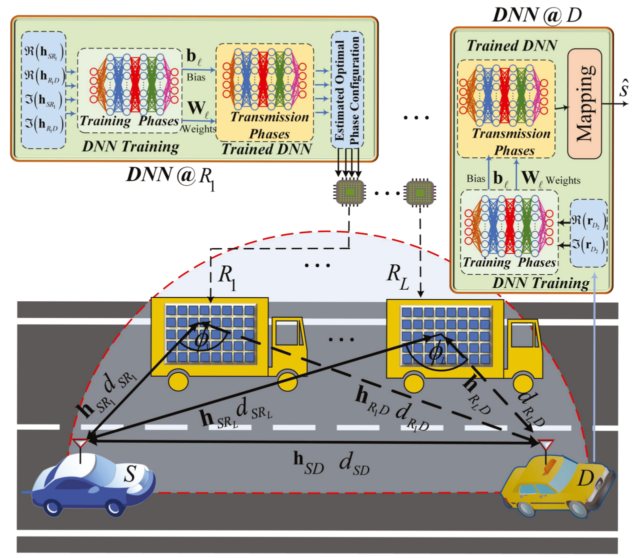

Fig. 1. System model of intervehicular communication through cascaded Nakagami-m and Nakagami-m fading channels with DNNs at R and D.

I. Introduction

High penetration loss and attenuation effects resulting from walls and other obstructions in modern urban environments are some of the most compelling challenges wireless network designers should face. For achieving the required data throughput capacities in the face of these challenges, next generation wireless network architectures mostly take advantage of the latest improvements in various diversity schemes, such as antenna diversity, cooperative relaying and reconfigurable intelligent surface (RIS). Among these, RIS is an emerging hardware technology, comprised of multiple passive electronic devices forming a reflecting surface, altering the phase angles of the incoming electromagnetic waves and reflecting with maximum strength. Initially conceived as an active frequency selective surface for indoor environments [1], this concept has also been adapted for outdoor scenarios and deployed on building exteriors.

The potential of RIS deployment in cooperative communications is an important research topic, involving the usage of single or multiple RIS-based relays (R) between source (S) and destination (D) nodes. Additionally, optimizing the RIS using deep-learning (DL) techniques is a novel approach already studied in various works which focus on symbol estimation [2], indoor signal focusing [3], or securing wireless communications [4] in stationary networks. In vehicular networks characterized by high-speed mobility elements, [5] explores efficient mobility and handover management to enable ultrareliable low-latency communications, employing various DL, reinforcement learning (RL), and deep reinforcement learning (DRL) techniques. In this context, [6] proposes a dynamic control scheme based on multi-agent DRL to maximize the uplink sum-rate of multi-RIS assisted multi-cell networks in mobility scenarios, treating base stations as independent agents. Nevertheless, the aforementioned works lack a symbol estimation mechanism based on a low complexity DL-based approach.

For multi-hop relaying or cooperative systems, most of the related literature focuses on the classical fading channels, such as Rayleigh, Rician, and Nakagami, to approximate the channel model, where S is stationary. Additionally, in studies investigating RIS-aided transmission for vehicles in motion, the involved channels are assumed to experience fast fading due to large Doppler spread, as seen in [7], while [8] deals with Rayleigh fading and [9] with Rician fading. However, none of these works address the intervehicular transmission environment characterized by cascaded Nakagami-m fading channels, already demonstrated to provide an accurate channel model in [10].

A significant challenge in RIS-assisted communication systems is the acquisition of channel state information (CSI), which most studies presume to have perfect knowledge of either at the RIS or the receiver. However, recent research, exemplified by [11], [12], and [13], have explored CSI estimation and feedback using DL techniques, showing promising outcomes and indicating new directions for future research.

A. Contributions

In our proposed work, we present a combination of DNN-assisted phase optimization and symbol detection schemes dealing with the effects introduced by cascaded Nakagami-m fading channels in an intervehicular network while also considering path loss effects. We can summarize the contributions of our paper as follows:

- In the proposed system model, DNNs are utilized at R and D within a cooperative network for phase optimization and symbol

Manuscript received 20 December 2023; revised 29 April 2024; accepted 11 June 2024. Date of publication 19 June 2024; date of current version 7 November 2024. This work was supported in part by the Scientific Research Projects Coordination of Yildiz Technical University under Project FBA-2023-5779 and in part by the Scientific and Technological Research Council of Turkey (TÜBİTAK) under Project 123E513. The review of this article was coordinated by Dr. Shaowei Wang. *(Corresponding author: Erdogan Aydin.)*

Bulent Sagir is with the Turk Telekomunikasyon A. S, Türkiye, and also with the Yıldız Technical University, Department of Electronics and Communications Engineering, 34349 Istanbul, Davutpasa, Türkiye (e-mail: bulent.sagir@turktelekom.com.tr).

Erdogan Aydin is with the Department of Electrical and Electronics Engineering, Istanbul Medeniyet University, 34857 Istanbul, Türkiye (e-mail: erdogan.aydin@medeniyet.edu.tr).

Haci Ilhan is with the Yıldız Technical University, Department of Electronics and Communications Engineering, 34349 Istanbul, Türkiye (e-mail: ilhanh@yildiz.edu.tr).

Digital Object Identifier 10.1109/TVT.2024.3416879

estimation, respectively, where the RISs are used as the sole relaying elements in a path-fading environment. The signals from multiple relays are combined at D, or alternatively, the best performing relay can be selected using relay selection (RS) schemes.
- Various scenarios, encompassing line-of-sight (LOS) and non-line-of-sight (nLOS) links, are explored, incorporating Nakagami-m and cascaded Nakagami-m fading channels to model intervehicular environments, with due consideration given to path loss effects.
- The performance of each scenario is thoroughly analyzed and compared in terms of bit error rate (BER), supplemented by a comprehensive computational complexity analysis. Notably, the proposed DNN-based models exhibit substantially lower complexities compared to conventional methods.

II. System Model

This section presents the generic model of intervehicular communication through a combination of cascaded Nakagami-m and Nakagami-m fading channels with DNNs at R and D.

The proposed system model is shown in Fig. 1, where S, D, and R operate in half duplex mode with a single pair of transmit and receive antennas. The distances d_{SR_ℓ}, $d_{R_\ell D}$ and d_{SD} represent the distances of S to ℓth R ($S \rightarrow R_\ell$), ℓth R to D ($R_\ell \rightarrow D$) and S to D ($S \rightarrow D$), respectively. Here, $\ell = 1, 2, \ldots, L$ where L is the number of relays in the system. In this configuration, ϕ_ℓ is the angle between $S \rightarrow R_\ell$ and $R_\ell \rightarrow D$ links, assuming $\pi/2 < \phi_\ell < \pi$ for all conditions, ensuring all relays stay within the half-circle area.

In our study, we investigate vehicle-to-vehicle communications where S and D communicate over a single LOS link assisted with nLOS links thanks to other vehicles in their vicinity or stationary roadside access points (AP) acting as relays in a cooperative scheme. Here, we evaluate two main scenarios: In the first scenario, it is assumed that all the channels in the transmission are subject to cascaded Nakagami-m fading, where the relaying is carried out by neighboring vehicles. In the second scenario, only the channel between S and D vehicles is modeled by cascaded Nakagami-m fading, whereas the remaining channels involving the stationary APs are modeled by Nakagami-m fading. We assume that each RIS is formed as a reflect-array incorporating N reconfigurable reflecting elements and used as a relay directing the signals from S to D in a cooperative network. In the literature, considering the wireless channel modeling with RIS deployments discussed in [14] and [15], S and D are positioned at a distance from R_ℓ, ensuring the nodes are not in the near-field region.

In our proposed model, for all the links, the path loss effect is proportional to d^{-c}, where d is the propagation distance, and c is the path loss exponent. The distance for the $S \rightarrow D$ link is conceived as unity, and the relative gains for $S \rightarrow R_\ell$ and $R_\ell \rightarrow D$ links can be expressed as $\mathcal{A}_{SR_\ell} = (d_{SD}/d_{SR_\ell})^c$ and $\mathcal{A}_{R_\ell D} = (d_{SD}/d_{R_\ell D})^c$ respectively, where $\mathcal{A}_{SR_\ell}$ and $\mathcal{A}_{R_\ell D}$ are correlated by law of cosines [16]. As d_{SR_ℓ} and ϕ_ℓ are given and $d_{SD} = 1$, $d_{R_\ell D}$ can be calculated and path loss can be applied to channel coefficients for $S \rightarrow R_\ell$ and $R_\ell \rightarrow D$ links. Thus, the channel vectors can be depicted as $\mathbf{h}_{SR_\ell} = [h_{SR_{\ell,1}}, h_{SR_{\ell,2}}, \ldots, h_{SR_{\ell,N}}] \in \mathbb{C}^{1\times N}$ and $\mathbf{h}_{R_\ell D} = [h_{R_{\ell,1}D}, h_{R_{\ell,2}D}, \ldots, h_{R_{\ell,N}D}] \in \mathbb{C}^{1\times N}$, where $\ell = 1, 2, \ldots, L$, and $\mathbb{C}$ represents the set of complex numbers. Here, it is possible to express the elements of the channel vectors for both channels in terms of channel amplitudes and phases, such as $h_{SR_{i,j}} = \alpha_{i,j} e^{-j\varphi_{i,j}}$ and $h_{R_{i,j}D} = \beta_{i,j} e^{-j\theta_{i,j}}$, respectively, where $i \in \{1, 2, \ldots, L\}$ and $j \in \{1, 2, \ldots, N\}$. In the first scenario, for $S \rightarrow D$, $S \rightarrow R_\ell$ and $R_\ell \rightarrow D$ cascaded Nakagami-m channels, the complex channel coefficients can be expressed as the product of statistically independent, but not necessarily identically distributed, two or more Nakagami random variables (RVs) such that, $h_{SD} = h_{SD_1} h_{SD_2} \ldots h_{SD_K}$, $h_{SR_\ell} = h_{SR_{\ell 1}} h_{SR_{\ell 2}} \ldots h_{SR_{\ell K}}$ and $h_{R_\ell D} = h_{R_\ell D_1} h_{R_\ell D_2} \ldots h_{R_\ell D_K}$, respectively, where the number of Nakagami RVs (K) determine the degree of cascading. As all the respective channel magnitudes follow the cascaded Nakagami-m distribution, the probability density function (PDF) can be expressed as

$$f_h(h) = \frac{2}{h \prod_{i=1}^{K} \Gamma(m_i)} G_{0,K}^{K,0} \left(h^2 \prod_{i=1}^{K} \frac{m_i}{\Omega_i} \Big|_{m_1,\ldots,m_K}^{-} \right), \quad (1)$$

where the subscripts SD, SR_ℓ and $R_\ell D$ are omitted for convenience. Here, $G_{0,K}^{K,0}(.| :)$ is the Meijer G-function and $\Gamma(.)$ is the Gamma function [10]. m_i is a parameter for the fading intensity given by $m_i = \Omega_i^2 / E[(h_i^2 - \Omega_i)^2] \geq 1/2$, with $\Omega_i = E[h_i^2]$ and $E[.]$ denoting the expectation operator.

In the second scenario, as $S \rightarrow R_\ell$ and $R_\ell \rightarrow D$ links are subject to Nakagami-m fading ($h_{SD_i}, h_{SR_{\ell i}}, h_{R_\ell D_i}, i \in \{1, 2, \ldots, K\}$), the PDF for the respective channel coefficients will be $f_h(h) = \frac{2m^m}{\Omega^m \Gamma(m)} h^{2m-1} \exp(-\frac{m}{\Omega} h^2)$.

The noisy received signal at D through $S \longrightarrow D$ cascade LOS link only, can be expressed as

$$r_{D,1} = \sqrt{E_s} h_{SD} s + n_1, \quad (2)$$

where s is the M-QAM modulated signal, $n_1 \sim \mathcal{CN}(0, \mathcal{N}_0)$ is the additive white Gaussian noise (AGWN) with zero mean, $\mathcal{N}_0/2$ is the variance per dimension at D and E_s is the average transmitted energy per symbol. The noisy signals received at D, through R_ℓ can be given as

$$\begin{aligned} r_{D,2_\ell} &= \sqrt{E_s \mathcal{A}_{SR_\ell} \mathcal{A}_{R_\ell D}} \left(\sum_{n=1}^{N} h_{SR_{\ell,n}} e^{j\phi_{\ell,n}} h_{R_{\ell,n}D} \right) s + n_\ell \\ &= \sqrt{E_s \mathcal{A}_{SR_\ell} \mathcal{A}_{\mathcal{A}_\ell D}} \left(\mathbf{h}_{SR_\ell} \mathbf{\Phi}_\ell \mathbf{h}_{R_\ell D}^T \right) s + n_\ell. \end{aligned} \quad (3)$$

Here, $\mathbf{\Phi}_\ell \triangleq \mathtt{diag}(\boldsymbol{\phi}_\ell) \in \mathbb{C}^{N\times N}$ is the diagonal phase matrix incorporating the adjusted phase angles for each RIS reflecting element, where the phase vector for ℓth RIS is $\boldsymbol{\phi}_\ell = [\phi_{\ell,1}, \phi_{\ell,2}, \ldots, \phi_{\ell,N}]$. The phase angles are adjusted for maximizing the signal strength at D, ensuring $\phi_{\ell,i} = \varphi_{\ell,i} + \theta_{\ell,i}$ for $i = 1, \ldots, N$. Finally, the vectorial representation of the noisy baseband signals reflected from all relays and received at D, can be given as $\mathbf{r} = [r_{D,2_1}, \ldots, r_{D,2_L}]^T \in \mathbb{C}^{L\times 1}$.

For the proposed system, the channel state information is assumed to be perfectly known at each relay, by utilizing fixed probes on various locations for pilot signal propagation.

III. Intelligent Transmission Model

In this section, we present an implementation framework for the proposed system model, which involves a signal combining scheme at D and utilizes DNN-based techniques for phase optimization at R and symbol estimation at D.

A. Combining Techniques at D

1) Relay Selection (RS): In the RS scheme, R with the lowest BER value is selected among L relays. The best relay selected for transmission can be given as

$$\widetilde{BER}_{\ell^*} = \arg\min_{\ell} \{BER_{D,2_1}, BER_{D,2_2}, \ldots, BER_{D,2_L}\}. \quad (4)$$

Here, $\ell = 1, 2, \ldots, L$. Also, ℓ^* represents the link having the lowest BER value among L relays [16].

2) Maximum Ratio Combining (MRC): In MRC scheme, the signals from multiple relays and $S \longrightarrow D$ link are combined at D. The combined signal at D can be given as

$$r_{\text{MRC}} = w_0 r_{D,1} + w_1 r_{D,2_1} + w_2 r_{D,2_2} + \cdots + w_L r_{D,2_L}, \quad (5)$$

where $r_{D,1}$ and $r_{D,2_\ell}$ are defined in (2) and (3), respectively. Here, the combining coefficients w_0 and w_ℓ are the conjugates of the complex channel coefficients to produce the sum of the absolute squared magnitudes of channel responses. Thus, the combining coefficients w_0 and w_ℓ for the $S \longrightarrow D$ and $S \longrightarrow R_\ell \longrightarrow D$ links can be expressed, respectively, as [16]

$$w_0 = (h_{SD})^*,$$
$$w_\ell = \left(\sum_{n=1}^{N} h_{SR_{\ell,n}} e^{j\phi_{\ell,n}} h_{R_{\ell,n}D}\right)^* = (\mathbf{h}_{SR_\ell} \mathbf{\Phi}_\ell \mathbf{h}_{R_\ell D}^T)^*. \quad (6)$$

Following the MRC-based combining at D, ML detector estimates the signal, which can be defined as

$$\hat{s}_{\text{MRC}} = \arg \min_{\upsilon \in \{1,2,\ldots,M\}} \left\{ \left| r_{\text{MRC}} - \left(w_0 h_{SD} + w_1 \sum_{n=1}^{N} h_{SR_{1,n}} e^{\hat{\phi}_{1,n}} h_{R_{1,n}D} + \cdots + w_L \sum_{n=1}^{N} h_{SR_{L,n}} e^{\hat{\phi}_{L,n}} h_{R_{L,n}D} \right) s_\upsilon \right|^2 \right\}, \quad (7)$$

where M represents the modulation order, and s_υ denotes all possible symbols to be transmitted for $\upsilon \in \{1, 2, \ldots, M\}$.

B. Proposed DNN-Based Relay and Destination Models

In this section, we will provide an overview of DNN assisted phase optimization and DNN-based symbol estimation techniques for the proposed model.

The DNNs are implemented at two critical stages in the model. At each R_ℓ, a DNN optimizes the phase vectors using channel coefficients for $S \longrightarrow R_\ell$ and $R_\ell \longrightarrow D$ links, and at D, another DNN estimates the symbols based on the received signals, which are exposed to path-fading and noise.

In the proposed scheme, the DNN process is split into two phases. First, the DNNs are trained with the training data set during the initial training phase, and then the trained DNNs are fed with real-world data to estimate the required parameters during the transmission phase. The training data set for the DNN at R_ℓ comprises channel coefficients $(\mathbf{h}_{SR_\ell}, \mathbf{h}_{R_\ell D})$ as feature vectors and respective phase vectors $(\boldsymbol{\phi}_\ell)$ as outputs for estimating the optimal phase vector that maximizes the signals reflected through the relays. During the transmission phase, new channel coefficients for $S \rightarrow R_\ell$ and $R_\ell \rightarrow D$ links are received by the DNN, and the DNN estimates the optimal phase vectors $(\hat{\boldsymbol{\phi}}_\ell)$ and transmits them to the RIS. The RIS elements use these phase estimations for the ongoing signal transmission until the channel conditions change and new channel coefficients arrive. On the other hand, the training data set for the DNN at D comprises the noisy and path-faded signals received at D as feature vectors and the respective modulated symbols (s) as outputs. During the transmission, the trained DNN estimates the symbols $(\hat{s})$ using the noisy signals received at D in real-time.

Both DNN models contain 4 hidden layers, 1 input and 1 output layer, where each hidden layer has 256 fully connected neurons. In both models, rectified linear unit (ReLU) activation function is deployed at hidden layers and can be expressed as $\sigma_{\text{ReLU}}(p) = \max(0, p)$, for a neuron with input p [16].

Defining the estimation process for DNN at D as a multiclass classification problem is crucial for mapping symbols to estimation classes. On the other hand, DNN at R is defined for regression. Consequently, the output layers of DNN at R and D will be configured as regression and classification layers to estimate complex phase adjustments $(\hat{\boldsymbol{\phi}}_\ell)$ and symbols $(\hat{s})$, respectively.

A classification layer is typically deployed after the softmax layer, which has the activation function $\sigma_{\text{softmax}}(\mathbf{p})_i = e^{p_i} / (\sum_{j=1}^{\mathcal{K}} e^{p_j})$. Here, $\mathbf{p}$ and p_i represent $\mathcal{K}$ vectors from the previous layer and the input vector elements, respectively, where $i = 1, \ldots, \mathcal{K}$ and $\mathbf{p} = (p_1, \ldots, p_k) \in \mathbb{R}^{\mathcal{K}}$ [16].

C. Generating Training Data Set and the Training Process

To train the proposed DNN at R, we need feature vectors $h_{SR_{\ell,n}}$ and $h_{R_{\ell,n}D}$ as input and adjusted phase angles $\boldsymbol{\phi}_\ell$ as output. Due to the processing constraints of the DNN, both input and output vectors should be separated into real and imaginary parts, respectively, as

$$\mathbf{U}_{\text{train}}^i = \left[\Re\left(h_{SR_{\ell,n}}\right) \; \Im\left(h_{SR_{\ell,n}}\right) \; \Re\left(h_{R_{\ell,n}D}\right) \; \Im\left(h_{R_{\ell,n}D}\right)\right]_{1\times 4}, \quad (8)$$

$$\mathbf{G}_{\text{train}}^i = \left[\Re\left(\phi_{\ell,n}\right) \; \Im\left(\phi_{\ell,n}\right)\right]_{1\times 2}. \quad (9)$$

Here, the feature vector $\mathbf{U}_{\text{train}} \triangleq \mathbf{U}_{\text{train}}^1, \mathbf{U}_{\text{train}}^2, \ldots, \mathbf{U}_{\text{train}}^f$ for f samples, $i = 1, 2, \ldots, f$ and $\mathbf{U}_{\text{train}}^i \in \mathbf{U}_{\text{train}}$, and output vector $\mathbf{G}_{\text{train}} \triangleq \mathbf{G}_{\text{train}}^1, \mathbf{G}_{\text{train}}^2, \ldots, \mathbf{G}_{\text{train}}^f$ for $i = 1, 2, \ldots, f$ and $\mathbf{G}_{\text{train}}^i \in \mathbf{G}_{\text{train}}$. Once we have feature and output vectors, training data set can be generated as

$$\mathcal{D}_{\text{train}} = \left\{\left\{\mathbf{U}_{\text{train}}^1, \mathbf{G}_{\text{train}}^1\right\}, \left\{\mathbf{U}_{\text{train}}^2, \mathbf{G}_{\text{train}}^2\right\}, \ldots, \left\{\mathbf{U}_{\text{train}}^f, \mathbf{G}_{\text{train}}^f\right\}\right\}. \quad (10)$$

The loss function for the proposed DNN architecture at R can be expressed as

$$\mathcal{L}(\Theta) = \frac{1}{2} \sum_{i=1}^{f} \left\| \boldsymbol{\phi}_{\ell,n}^i - \hat{\boldsymbol{\phi}}_{\ell,n}^i(\Theta) \right\|^2, \quad (11)$$

where $\boldsymbol{\phi}_{\ell,n}$ is the desired output value, $\hat{\boldsymbol{\phi}}_{\ell,n}$ is the estimated output, and i denotes the response index. Here, Θ represents the training parameter set as $\Theta \triangleq \{\boldsymbol{\varpi}_1, \boldsymbol{\varpi}_2, \ldots, \boldsymbol{\varpi}_f\}$ with $\boldsymbol{\varpi}_k \triangleq \{\mathbf{W}_k, \mathbf{b}_k\}$, consisting of weight and bias values of the kth layer, respectively.

For the proposed DNN at D, the estimator should converge to the nearest $\hat{s}$ for the original symbol. During the process, $\hat{s}$ will be selected from a symbol set $\mathbb{S}$, which is basically mapped onto a class set C, both of which can be defined as

$$\mathbb{S} = \{s_{\mathbb{S}_1}, s_{\mathbb{S}_2} \ldots, s_{\mathbb{S}_M}\}, C = \{\mathbb{Y}_1, \mathbb{Y}_2, \ldots, \mathbb{Y}_M\}, \quad (12)$$

for Mth modulation order. Here, C represents the set of class labels mapped to each element of the symbol set $\mathbb{S}$, where $s_{\mathbb{S}_\upsilon} \in \mathbb{S}$ and $\mathbb{Y}_\upsilon \in C$ for $\upsilon = 1, 2, \ldots, M$. Mapping relation between $\mathbb{S}$ and C can be represented by $\{s_{\mathbb{S}_\upsilon} \longleftrightarrow \mathbb{Y}_\upsilon\} \longrightarrow \hat{s}_f$. Finally, the feature vector and the respective output vector can be defined as

$$\mathbf{U}_{\text{train}}^i = \left[\Re(r_{D,2_\ell}), \Im(r_{D,2_\ell})\right]_{1\times 2}, \; \mathbf{G}_{\text{train}}^i = \left[\mathbb{Y}_\upsilon^i\right]_{1\times 1}, \quad (13)$$

where $\mathbf{r}_{\ell,n}$ is separated into real and imaginary parts as in (8) for $i = 1, 2, \ldots, f$, and $\mathbb{Y}_\upsilon$ is a class category for $\mathbf{G}_{\text{train}}^i$. Hence, the training data set can be formed as in (10) with feature vector and class pairs for the sample space f.

TABLE I
TRAINING PARAMETERS

Training Parameter	DNN@Relay	DNN@Destination
Modulation Order (M)	4	
Num. of Tx and Rx Antennas	1	
Num. of Reflect. Elements (N)	8/16/32	
Path Loss Exponent (c)	4	
Num. of Hidden Layers	4	
Batch Size	256	
Validation Split	10%	
Num. of Samples (s)	400000	50000
Iteration Steps	600	400
Learning Rate (η)	0.003	0.003

Algorithm 1: Training Algorithm for DNNs.

Input: Feature vectors for DNNs ($\mathbf{h}_{SR_\ell}, \mathbf{h}_{R_\ell D}$ and $\mathbf{r}$).
Output: Trained DNNs.
Initialisation: Training parameters ($\mathbf{W}_k$, $\mathbf{b}_k$) and $\mathcal{L}(\Theta)$ are set to zero.
LOOP Process
1: **for** $i = 1$ to s **do**
2: Process feature vectors to generate $\mathbf{U}^i_{\text{train}}$ as in (8), (13).
3: Compute output vector elements ($\boldsymbol{\phi}_{\ell,n}$, $\mathbb{S}$, $\mathcal{C}$) as in (12).
4: Generate output vector $\mathbf{G}^i_{\text{train}}$ for DNNs as in (9), (13).
5: **end for**
6: Generate training dataset D_{train} as in (10) for DNNs.
7: Train DNNs until $\mathcal{L}(\Theta)$ is minimized with respect to (11) and (14).
8: **return** Trained DNNs.

The loss function for the DNN at D can be expressed as

$$\mathcal{L}(\Theta) = -\frac{1}{f}\sum_{i=1}^{f}\sum_{\upsilon=1}^{M} \mathbb{Y}^i_\upsilon \ln \hat{\mathbb{Y}}^i_\upsilon(\Theta). \tag{14}$$

Here, f represents the number of samples, M is the number of classes, $\mathbb{Y}^i_\upsilon$ is the desired value for the υth class at ith sample, and $\hat{\mathbb{Y}}^i_\upsilon$ is the actual output value [16].

The theoretical training algorithm for DNN at R_ℓ and DNN at D is given in Algorithm 1.

IV. NUMERICAL RESULTS AND DISCUSSIONS

A. Simulation Parameters

The simulation is realized for phase optimization at R and symbol estimation at D. In the simulation, S, R_ℓ, and D are located as shown in Fig. 1, and all relays are positioned over the half circle area by the relation $\pi/2 < \phi_\ell < \pi$, where d_{SD}, d_{SR_ℓ}, and $d_{R_\ell D}$ distances are normalized with respect to $d_{SD} = 1$. The signal to noise ratio (SNR) used in the simulations can be given as $\text{SNR(dB)} = 10\log_{10}(E_s/N_0)$. All Nakagami-$m$ and cascaded Nakagami-m fading channels are modeled regarding path loss effects with $c = 4$, indicating a dense urban environment [16].

Simulation is realized in the MATLAB environment using the training parameters given in Table I. During training, validation split determines the percentage of training data reserved for validation process, and set as 10% with the validation frequency of 10 for both DNNs. Batch size is set as 256 for both DNN models, and defines the size of the data batch to be processed on each training iteration. During the simulation, to evaluate the generalization ability of the proposed DNNs, completely different sets of channel coefficients and SNR ranges are used in the training and transmission phases. It is found that the general accuracy level improves with the increase in SNR as expected, and the algorithm produces nearly identical results for different training and transmission conditions.

B. BER Performance Analysis

The performances of the proposed DNN-based systems are evaluated in terms of BER using various configurations with variable N, K, and m values to realize the impact of these parameters on the general performance. For all the scenarios, a two relay system is considered with $d_{SR_1} = 0.5$ and $d_{SR_2} = 0.7$ where RS scheme is applied at D unless otherwise stated.

In Fig. 2(a), the BER performances are presented for scenario 1, where all channels undergo cascaded Nakagami-m fading with $K = 2$ and $m = 3$, while varying the number of RIS reflecting elements (N) for relay configurations of 8, 16, and 32 elements, with other parameters held constant. As expected, increasing N leads to substantial performance gains of up to 15 dB across all relay configurations, due to the enhanced signal diversity.

Notably, the performance of combined DNN-assisted phase and symbol estimation closely matches that of non-DNN or relay-only DNN configurations across varying RIS sizes. Given that the training data is based on non-DNN techniques and integrates phase adjustments derived from the theoretical background outlined earlier, this consistency in BER performance underscores the efficacy of the trained DNNs in these specific estimation tasks.

The effect of the cascading degree (K) is depicted in Fig. 2(b), where performance degrades with increasing K, resulting in an SNR loss of nearly 6 dB per cascading at a BER level of 10^{-3}. Similarly, Fig. 2(c) illustrates the effect of the Nakagami fading parameter (m), depicting a positive correlation between BER and m. Notably, the performance of the combined DNN-based R and D scheme remains unaffected by variations in K or m, demonstrating consistency comparable to non-DNN configurations.

Finally, BER performances for the scenario 2 is shown in Fig. 3, for 8, 16, and 32 reflecting elements. We can observe the similar SNR gains with the increase in N as seen in the first scenario, but with a better overall performance as the cascading is effective only on the $S \rightarrow D$ link. Compared to the first scenario, the performance gap between DNN-based and non-DNN-based configurations is still marginal, but the RS performances are a bit closer to MRC, thanks to the increased N.

C. Complexity Analysis

Here, we present an analysis and comparison of the computational complexities of RS and MRC based receivers against the DNN-assisted symbol detection algorithm.

To analyze the DNN model, we consider the number of operations in each layer. In a multi-layer neural network, the complexity changes with the number and size of the layers, affecting the number of vector multiplications. Thus, for a multi-layer network with $\mathcal{K}$ fully connected hidden layers and p inputs, if the kth layer has n_k neurons with o neurons at the output, the total number of multiplications will be [16]

$$\mathcal{O}\left(pn_1 + n_{\mathcal{K}}o + \sum_{k=1}^{\mathcal{K}-1} n_k n_{k+1}\right). \tag{15}$$

Table II presents the computational complexities of RS, MRC, and DNN-based systems, along with the total number of real multiplications (RMs), considering a realistic deployment scenario with $L = 24$, $M =$

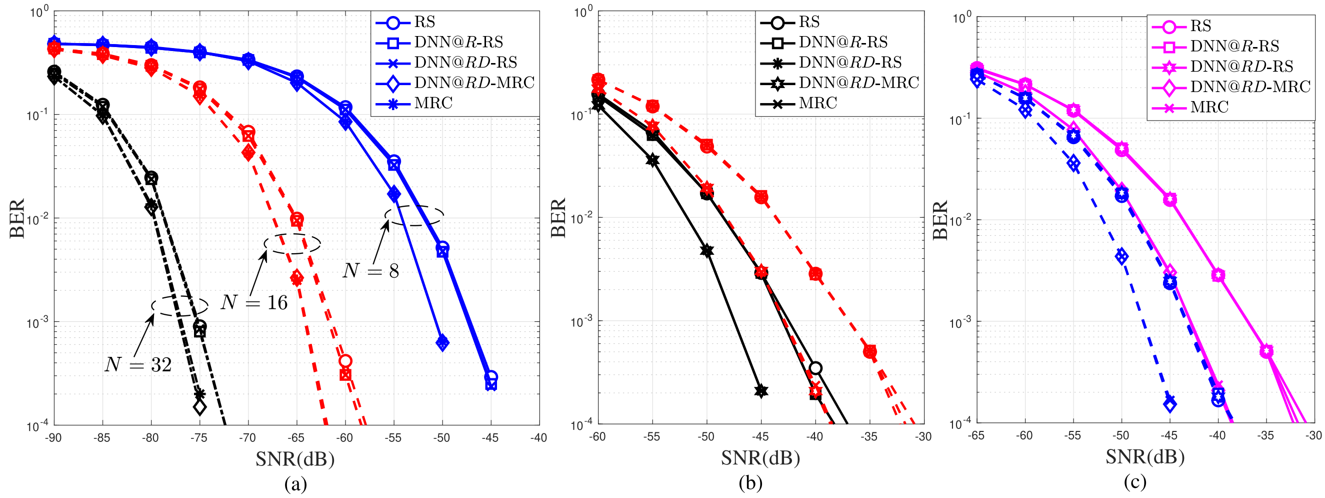

Fig. 2. BER comparisons of scenario 1 schemes for (a) $N = 8, 16, 32$, $K = 2$, $m = 3$, (b) $K = 2$ (continuous black line), 3 (dashed red line), $N = 8$, $m = 3$, (c) $m = 2$ (continuous cyan line), 3 (dashed blue line), $K = 3$, $N = 8$.

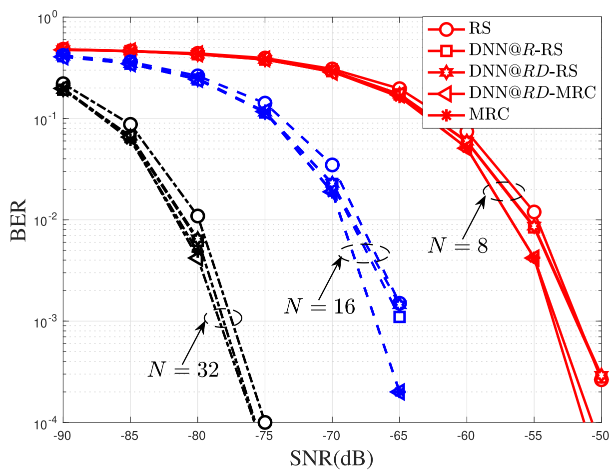

Fig. 3. BER comparisons of scenario 2 schemes for $N = 8, 16, 32$, $m = 3$, $K = 2$ for $S \rightarrow D$, $K = 1$ for $S \rightarrow R_\ell$ and $R_\ell \rightarrow D$.

TABLE II
COMPUTATIONAL COMPLEXITY ANALYSIS AND NUMBER OF RMS

Scheme	Complexity	RMs
RS	$O(N + 4M)$	192
MRC	$O(L(N+1) + 1 + 8M)$	3225
DNN@RD-RS	$O\left(pn_1 + n_{\mathcal{K}}o + \sum_{k=1}^{\mathcal{K}-1} n_k n_{k+1}\right)$	80
DNN@RD-MRC	$O\left(L(N+1) + 1 + pn_1 + n_{\mathcal{K}}o + \sum_{k=1}^{\mathcal{K}-1} n_k n_{k+1}\right)$	3177

16, $N = 128$, $\mathcal{K} = 2$, and $n_1 = n_2 = 8$. Given that the complexity of a DNN depends on its layer and neuron configurations, it is observed that complexity reduction is achievable without significant compromise on accuracy, particularly with 2 hidden layers. Consequently, both 2 and 4-layer networks exhibit nearly identical accuracy rates across a broad range of SNR levels, as indicated in Table III. Notably, the 2-layer DNN configuration demonstrates the lowest complexity compared to conventional methods configured with a high number of network components

TABLE III
ACCURACY COMPARISON OF 2-LAYER AND 4-LAYER DNNS ACROSS VARIED SNR LEVELS

SNR(dB)	2-Layer DNN	4-Layer DNN
-30	71.3%	72.1%
-40	39.9%	40.1%
-50	29.4%	29.5%

Besides the number of RMs, the complexity of the proposed DNN can also be analysed in terms of floating point operations (FLOPs). FLOPs encompass all arithmetic operations performed within a neuron, including input and output connections as well as bias additions. It can be calculated for the proposed DNN with $\mathcal{K}$ fully connected hidden layers with [17]

$$FLOPs = (2p + 1)n_1 + (2n_{\mathcal{K}} + 1)o + \sum_{k=1}^{\mathcal{K}-1}(2n_k + 1)n_{k+1}. \quad (16)$$

Utilizing (16) and the parameters specified for the same system configuration, the FLOPs can be computed for DNN-based symbol detection with RS and MRC as 386 and 3589, respectively.

V. CONCLUSIONS AND FUTURE WORKS

In this paper, we realize a DNN-assisted cooperative RIS scheme with DNN-based phase and symbol estimators at R and D, respectively, for intervehicular communication over Nakagami-m and cascaded Nakagami-m fading channels. Regarding the results of BER performance and complexity analyses, proposed DNN-based phase and symbol estimation models have shown exceptional performance in a range of communication scenarios, demonstrating significant performance gains with increasing N, while exhibiting similar BER performance compared to conventional models with much lower complexity.

While our proposed design demonstrates promising results, it's important to acknowledge potential implementation complexities in large-scale intervehicular networks, particularly concerning CSI acquisition and feedback. Given our model's reliance on perfect channel knowledge, future research directions could involve integrating CSI estimation methods with current DL-based techniques to mitigate reliance on perfect CSI knowledge. Another noteworthy consideration is the validation of the results using real-world data. Experimental validation in real-world scenarios could provide valuable insights into assessing the performance and practical applicability of the proposed model.

References

[1] S. Hu, F. Rusek, and O. Edfors, "Beyond massive MIMO: The potential of data transmission with large intelligent surfaces," *IEEE Trans. Signal Process.*, vol. 66, no. 10, pp. 2746–2758, May 2018.

[2] S. Khan and S. Y. K. Shin, "Deep-learning-aided detection for reconfigurable intelligent surfaces," 2020, *arXiv:1910.09136*.

[3] C. Huang, G. C. Alexandropoulos, C. Yuen, and M. Debbah, "Indoor signal focusing with deep learning designed reconfigurable intelligent surfaces," in *Proc. 20th IEEE Int. Workshop Signal Process. Adv. Wireless Commun.*, 2019, pp. 1–5.

[4] H. Yang, Z. Xiong, J. Zhao, D. Niyato, L. Xiao, and Q. Wu, "Deep reinforcement learning-based intelligent reflecting surface for secure wireless communications," *IEEE Trans. Wireless Commun.*, vol. 20, no. 1, pp. 375–388, Jan. 2021.

[5] J. Du, C. Jiang, J. Wang, Y. Ren, and M. Debbah, "Machine learning for 6G wireless networks: Carrying forward enhanced bandwidth, massive access, and ultrareliable/low-latency service," *IEEE Veh. Technol. Mag.*, vol. 15, no. 4, pp. 122–134, Dec. 2020.

[6] J. Kim, S. Hosseinalipour, T. Kim, D. J. Love, and C. Brinton, "Exploiting multiple intelligent reflecting surfaces in multi-cell uplink MIMO communications," 2020, *arXiv:2011.01141*.

[7] E. Basar, "Reconfigurable intelligent surfaces for doppler effect and multipath fading mitigation," *Front. Commun. Netw.*, vol. 2, 2021.

[8] Y. U. Ozcan, O. Ozdemir, and G. K. Kurt, "Reconfigurable intelligent surfaces for the connectivity of autonomous vehicles," *IEEE Trans. Veh. Technol.*, vol. 70, no. 3, pp. 2508–2513, Mar. 2021.

[9] Y. Chen, Y. Wang, J. Zhang, P. Zhang, and L. Hanzo, "Reconfigurable intelligent surface (RIS)-aided vehicular networks: Their protocols, resource allocation, and performance," *IEEE Veh. Technol. Mag.*, vol. 17, no. 2, pp. 26–36, Jun. 2022.

[10] H. Ilhan, M. Uysal, and I. Altunbas, "Cooperative diversity for intervehicular communication: Performance analysis and optimization," *IEEE Trans. Veh. Tech.*, vol. 58, no. 7, pp. 3301–3310, Sep. 2009.

[11] S. Zhang, S. Zhang, F. Gao, J. Ma, and O. A. Dobre, "Deep learning optimized sparse antenna activation for reconfigurable intelligent surface assisted communication," *IEEE Trans. Commun.*, vol. 69, no. 10, pp. 6691–6705, Oct. 2021.

[12] M. Liu, X. Li, B. Ning, C. Huang, S. Sun, and C. Yuen, "Deep learning-based channel estimation for double-RIS aided massive MIMO system," *IEEE Wireless Commun. Lett.*, vol. 12, no. 1, pp. 70–74, Jan. 2023.

[13] J. Guo, W. Chen, C.-K. Wen, and S. Jin, "Deep learning-based two-timescale CSI feedback for beamforming design in RIS-assisted communications," *IEEE Trans. Veh. Technol.*, vol. 72, no. 4, pp. 5452–5457, Apr. 2023.

[14] E. Basar and I. Yildirim, "Reconfigurable intelligent surfaces for future wireless networks: A channel modeling perspective," *IEEE Wireless Commun.*, vol. 28, no. 3, pp. 108–114, Jun. 2021.

[15] H. Jiang, B. Xiong, H. Zhang, and E. Basar, "Hybrid far- and near-field modeling for reconfigurable intelligent surface assisted V2V channels: A sub-array partition based approach," *IEEE Trans. Wireless Commun.*, vol. 22, no. 11, pp. 8290–8303, Nov. 2023.

[16] B. Sagir, E. Aydin, and H. Ilhan, "Deep-learning-assisted IoT-based RIS for cooperative communications," *IEEE Internet Things J.*, vol. 10, no. 12, pp. 10471–10483, Jun. 2023.

[17] C. Patel et al., "DBGC: Dimension-based generic convolution block for object recognition," *Sensors*, vol. 22, no. 5, 2022, Art. no. 1780.